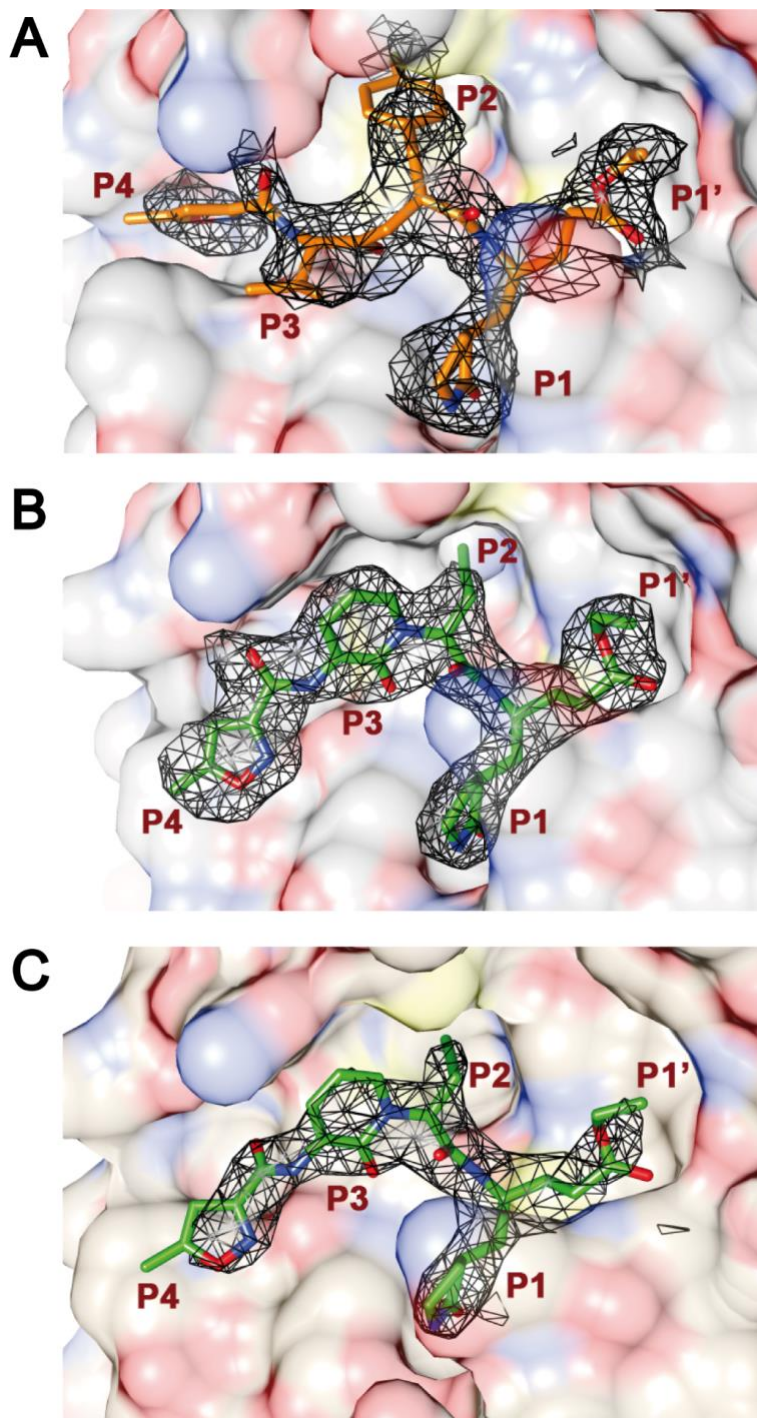


## **SUPPLEMENTARY FIGURES AND TABLES**

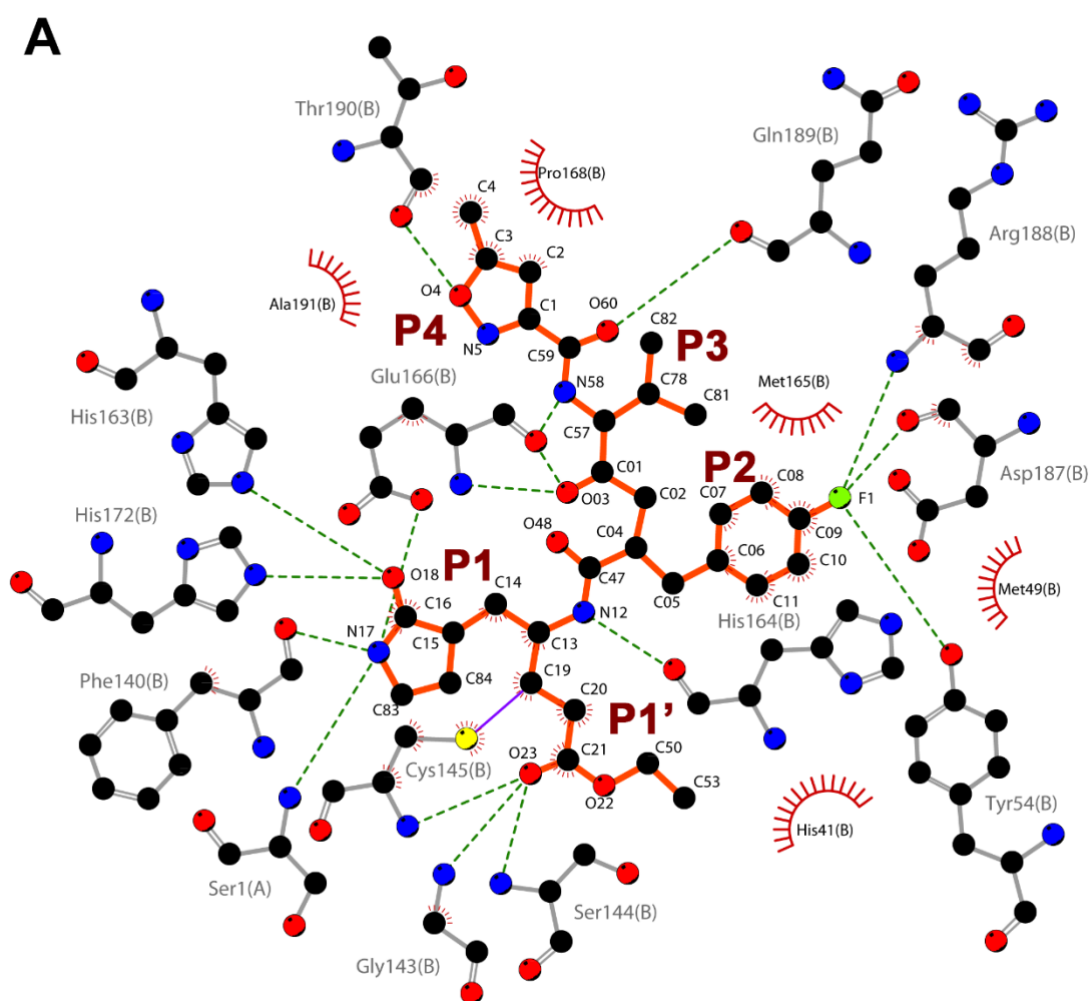
### **Structure and inhibition of SARS-CoV-1 and SARS-CoV-2 main proteases by oral antiviral compound AG7404.**

Montserrat Fàbrega-Ferrer, Alejandra Herrera-Morandé, Sara Muriel-Goñi, Julia Pérez-Saavedra, Paula Bueno, Victoria Castro, Urtzi Garaigorta, Pablo Gastaminza and Miquel Coll.

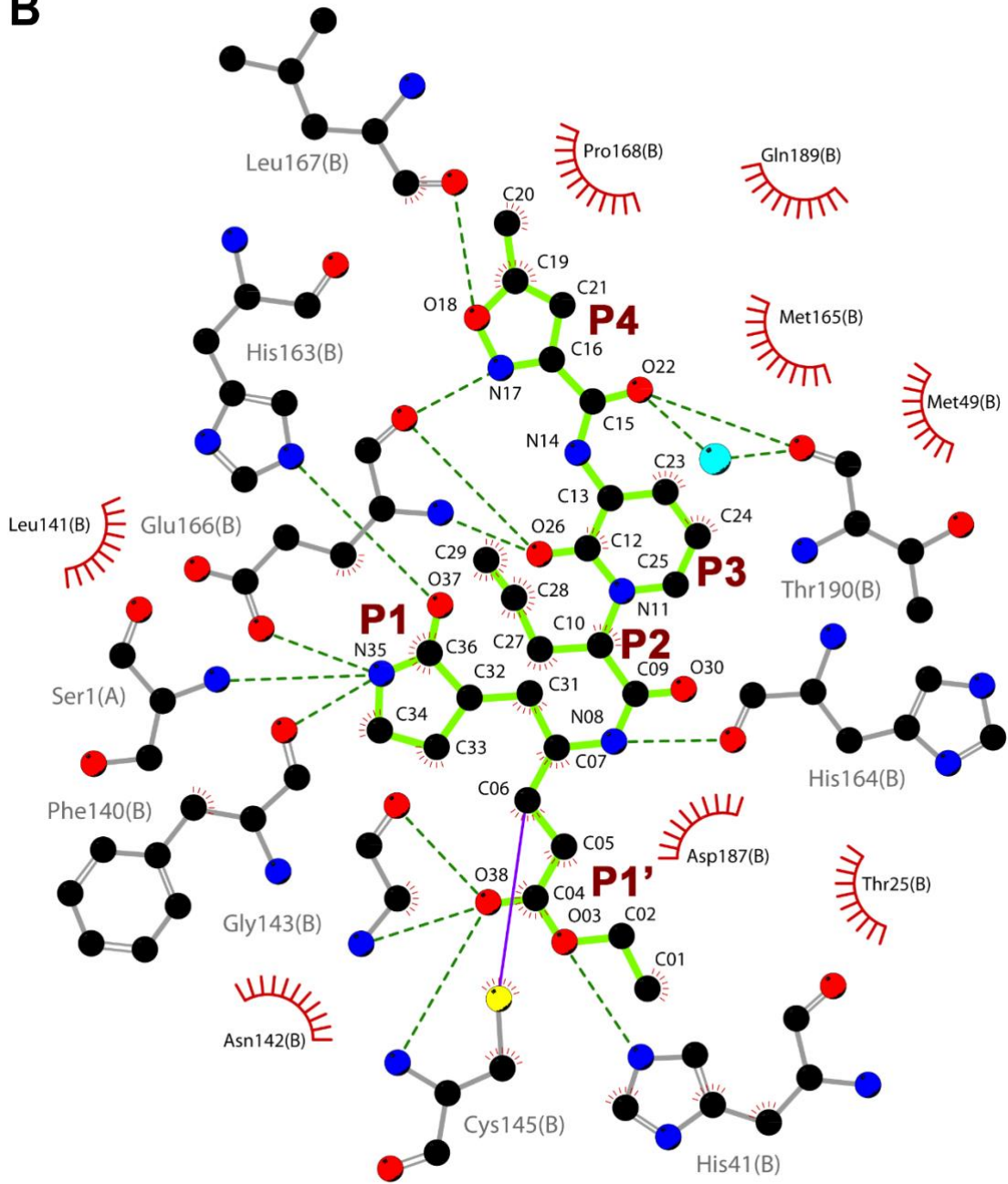
**Supplementary figure 1.  $2F_o-F_c$  electron density maps of the inhibitors.** (A) SARS-CoV-2  $M^{pro}$  with rupintrivir. (B) SARS-CoV-2  $M^{pro}$  with AG7404 1. (C) SARS-CoV-1  $M^{pro}$  with AG7404. Rupintrivir is shown in orange and AG7404 in lime green. Electron density around the compounds is depicted as a black mesh. Proteins are shown as atom-colored surface, the surface of SARS-CoV-2  $M^{pro}$  in gray and the surface of SARS-CoV-1  $M^{pro}$  in wheat. Subsites from P4 to P1' are also labeled.



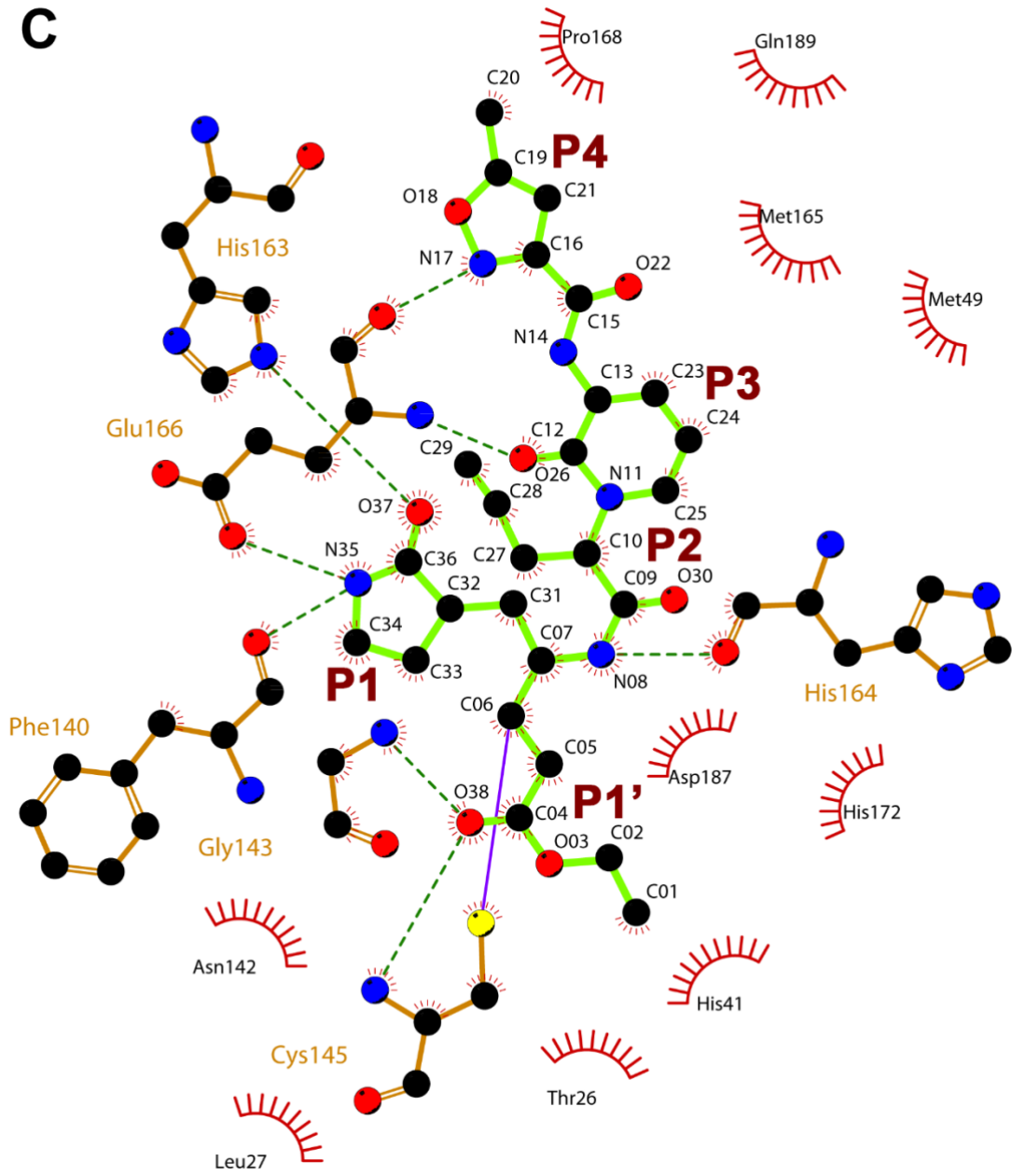
**Supplementary figure 2. Diagrams of inhibitor-target interactions.** (A) SARS-CoV-2 M<sup>pro</sup> with rupintrivir. (B) SARS-CoV-2 M<sup>pro</sup> with AG7404. (C) SARS-CoV-1 M<sup>pro</sup> with AG7404. Figures were obtained with LigPlot+ (Laskowski and Swindells, 2011). SARS-CoV-2 M<sup>pro</sup> is represented in gray, SARS-CoV-1 M<sup>pro</sup> in wheat, rupintrivir in orange, and AG7404 in lime green. Discontinuous green lines indicate hydrogen bonds and red spline curves show ligand atoms and protein residues that participate in hydrophobic contacts. Subsites from P4 to P1' are also labeled.



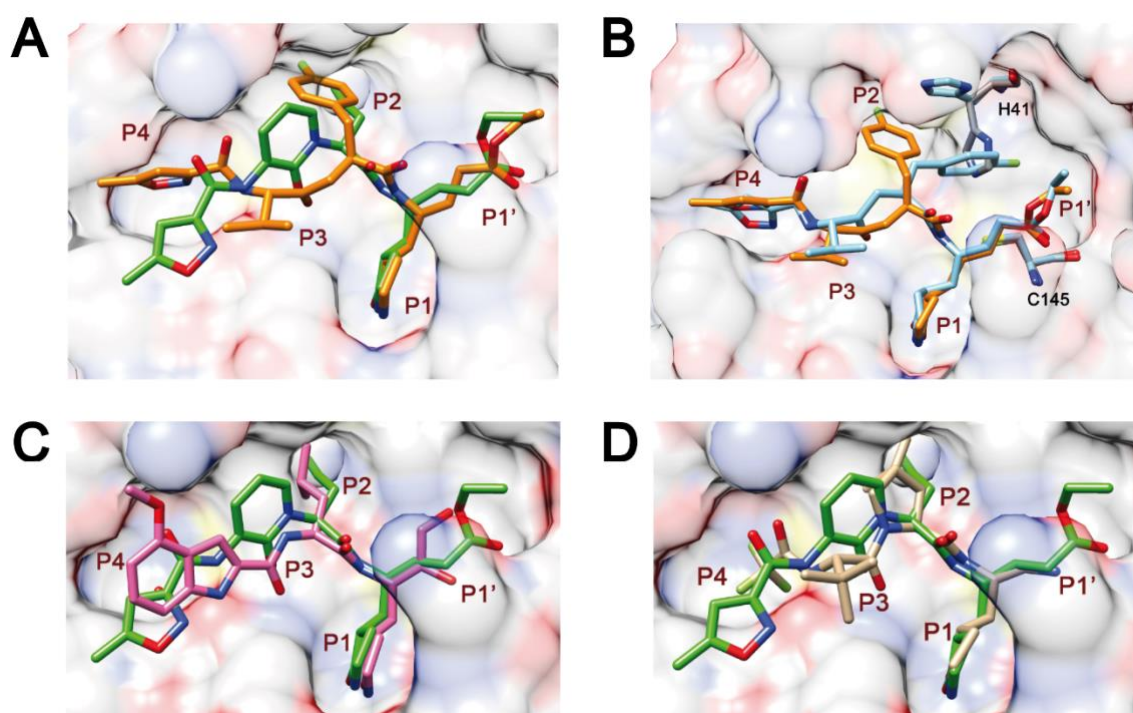
**B**



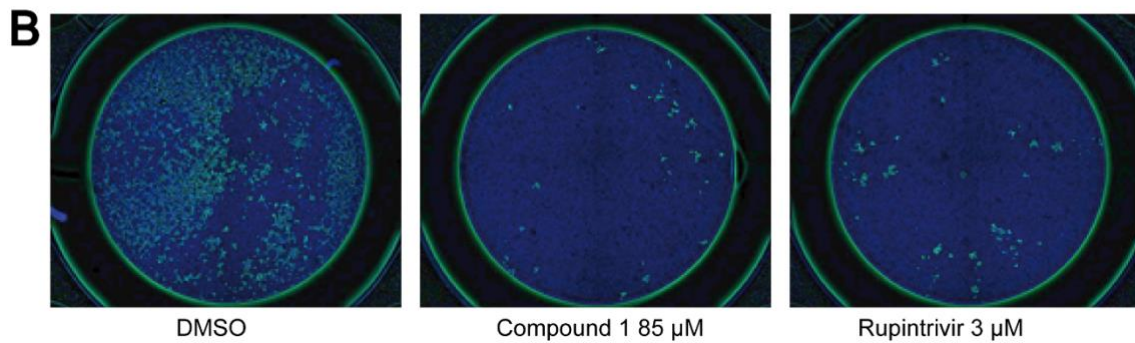
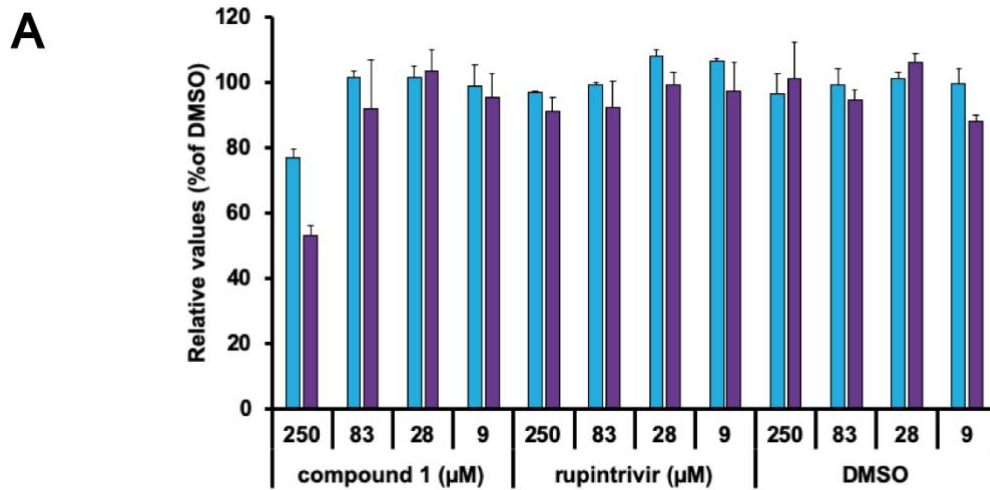
C



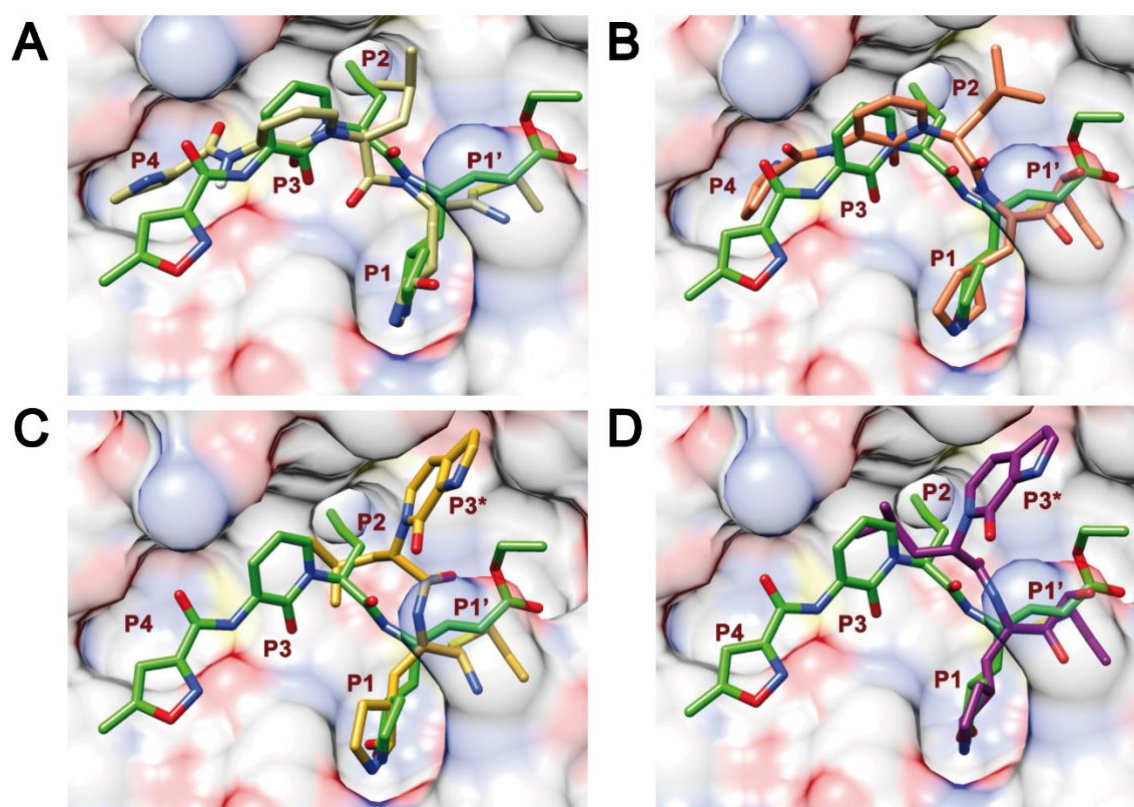
**Supplementary figure 3. Structure superpositions.** (A) Structures of SARS-CoV-2 M<sup>pro</sup> - AG7404 and SARS-CoV-2 M<sup>pro</sup> rupintrivir superposed. AG7404 is depicted in lime green and rupintrivir in orange. (B) SARS-CoV-2 M<sup>pro</sup> - rupintrivir structure (this study) superposed with a previously published structure (PDB 7L8I, Lockbaum et al., 2021). Rupintrivir presented in this paper is shown in orange, while the residues of the catalytic dyad are represented in gray. Rupintrivir and the catalytic dyad from the PDB 7L8I structure are depicted in blue. Note the displacement of the catalytic His41 in the PDB 7L8I structure. (C) Structures of SARS-CoV-2 M<sup>pro</sup> - AG7404 and SARS-CoV-2 M<sup>pro</sup> - PF-00835231 (PDB 6XHM, Hoffman et al., 2020) superposed. AG7404 is depicted in lime green and PF-00835231 in pink. (D) Structures of SARS-CoV-2 M<sup>pro</sup> - AG7404 and SARS-CoV-2 M<sup>pro</sup> - nirmatrelvir (PDB 7TLL, Greasley et al., 2022) superposed. AG7404 is depicted in lime green and nirmatrelvir in tan. For all panels, only the active site is shown with the protein depicted as atom-colored surface and subsites from P4 to P1' are labeled.



**Supplementary figure 4. Cellular assays.** (A) MTT cytotoxicity assay performed with AG7404, rupintrivir and a DMSO vehicle control. Purple bars indicate mitochondrial activity and blue bars correspond to the cell count per well. (B) Immunofluorescence microscopy images showing relative infection efficiency in cell culture. SARS-CoV-2 N protein is shown in green and nuclei in blue.



**Supplementary figure 5. Covalent docking of designed inhibitors.** (A) Inhibitor 1 (dark khaki). (B) Inhibitor 2 (choral). (C) Inhibitor 3 (goldenrod). (D) Inhibitor 4 (magenta). For all panels only the active site is shown, with lime green AG7404 crystal structure superposed for the sake of comparison. The protein is depicted as an atom-colored surface. Subsites from P4 to P1' are labeled and in (C) and (D) P3\* indicates the compound moiety designed to occupy the S3 subsite that is placed elsewhere by docking simulations.



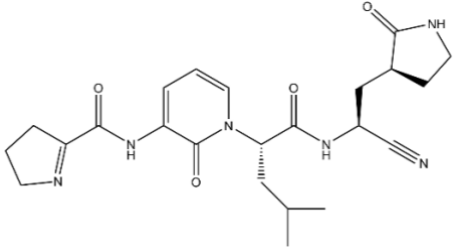
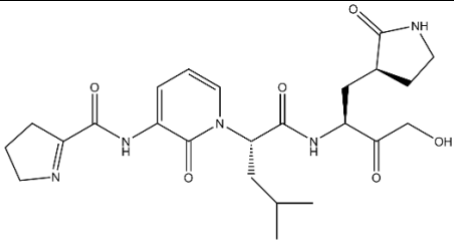
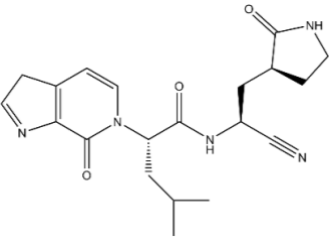
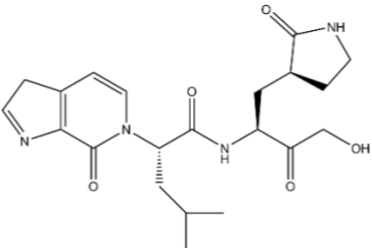


**Supplementary table 1.** Hydrogen bonds between the protein and the compounds. Cells shaded in gray correspond to inhibitor regions not well defined in electron density maps. For atom numbering of the inhibitors, please check Supplementary figure 1.

	<b>SARS-CoV-2 M<sup>pro</sup> AG7404</b>	<b>SARS-CoV-1 M<sup>pro</sup> AG7404</b>	<b>SARS-CoV-2 M<sup>pro</sup> Rupintrivir</b>
<b>P4</b>	AG7404 O18 Leu167 O 3.5 Å		Rupintrivir O4 Thr190 O 2.9 Å
	AG7404 N17 Glu166 O 3.4 Å	AG7404 N17 Glu166 O 3.3Å	
	AG7404 O22 Thr190 O 3.4Å		Rupintrivir O60 Gln189 Oε 3.2 Å
	AG7404 O22 Thr190 O Water mediated		
	AG7404 O22 Thr190 N Water-mediated		
<b>P3</b>			Rupintrivir N58 Glu166 O 2.7 Å
	AG7404 O26 Glu166 N 3.3 Å	AG7404 O26 Glu166 N 3.4Å	Rupintrivir O3 Glu166 N 2.8 Å
	AG7404 O26 Glu166 O 3.4 Å		Rupintrivir O3 Glu166 O 3.1 Å
<b>P2</b>			Rupintrivir F1 Tyr54 OH 3.3 Å
			Rupintrivir F1 Asp187 O 2.3 Å
			Rupintrivir F1 Arg188 N 2.7 Å

<b>P1</b>	AG7404 N8 His164 O 2.8 Å	AG7404 N8 His164 O 2.8 Å	Rupintrivir N12 His164 O 3.3 Å
	AG7404 N35 Phe140 O 2.9 Å	AG7404 N35 Phe140 O 3.1 Å	Rupintrivir N17 Phe140 O 2.9Å
	AG7404 N35 Glu166 Oε 3.1 Å	AG7404 N35 Glu166 Oε 2.9 Å	Rupintrivir N17 Glu166Oε 2.9 Å
	AG7404 N35 Ser1 N (Chain A) 3.3 Å		Rupintrivir N17 Ser1 N (Chain A) 3.4 Å
	AG7404 O37 His163 Nε 2.8Å	AG7404 O37 His163 Nε 2.6Å	Rupintrivir O18 His163 Nε 2.8 Å
			RupintrivirO18 His172Nε 3.5Å
<b>P1'</b>	AG7404 O38 Gly143 N 3.4 Å	AG7404 O38 Gly143 N 3.4 Å	Rupintrivir O23 Gly143 N 3.0 Å
	AG7404 O38 Gly143 O 3.3 Å		Rupintrivir O23 Ser144 N 3.4 Å
	AG7404 O38 Cys145 N 3.4 Å	AG7404 O38 Cys145 N 3.3 Å	Rupintrivir O23 Cys145 N 3.3 Å
	AG7404 O3 His41 Nε 3.4 Å		

**Supplementary table 2.** Structure-based design of inhibitors. The first column shows the compound numbers, the second one depicts their chemical structures and the third one shows their binding energy in docking simulations.

Compound no.	Chemical structure	Binding energy (kcal/mol) <sup>1</sup>
1		-9.3
2		-10.1
3		-8.9
4		-9.4

<sup>1</sup>Binding energies correspond to the AutoDockFR best cluster for each compound.

## SUPPLEMENTARY REFERENCES

- Greasley, S.E., Noell, S., Plotnikova, O., Ferre, R., Liu, W., Bolanos, B., Fennell, K., Nicki, J., Craig, T., Zhu, Y., Stewart, A.E., Steppan, C.M., 2022. Structural basis for the in vitro efficacy of nirmatrelvir against SARS-CoV-2 variants. *J. Biol. Chem.* 298, 101972. <https://doi.org/10.1016/j.jbc.2022.101972>
- Hoffman, R.L., Kania, R.S., Brothers, M.A., Davies, J.F., Ferre, R.A., Gajiwala, K.S., He, M., Hogan, R.J., Kozminski, K., Li, L.Y., Lockner, J.W., Lou, J., Marra, M.T., Mitchell, L.J., Murray, B.W., Nieman, J.A., Noell, S., Planken, S.P., Rowe, T., Ryan, K., Smith, G.J., Solowiej, J.E., Steppan, C.M., Taggart, B., 2020. Discovery of Ketone-Based Covalent Inhibitors of Coronavirus 3CL Proteases for the Potential Therapeutic Treatment of COVID-19. *J. Med. Chem.* 63, 12725–12747. <https://doi.org/10.1021/acs.jmedchem.0c01063>
- Laskowski, R.A., Swindells, M.B., 2011. LigPlot+: Multiple ligand-protein interaction diagrams for drug discovery. *J. Chem. Inf. Model.* 51, 2778–2786. <https://doi.org/10.1021/ci200227u>
- Lockbaum, G.J., Henes, M., Lee, J.M., Timm, J., Nalivaika, E.A., Thompson, P.R., Kurt Yilmaz, N., Schiffer, C.A., 2021. Pan-3C Protease Inhibitor Rupintrivir Binds SARS-CoV-2 Main Protease in a Unique Binding Mode. *Biochemistry* 60, 2925–2931. <https://doi.org/10.1021/acs.biochem.1c00414>